




## Article

# Coded Excitation for Crosstalk Suppression in Multi-line Transmit Beamforming: Simulation Study and Experimental Validation

Ling Tong <sup>1</sup>, Qiong He <sup>1</sup>, Alejandra Ortega <sup>2</sup>, Alessandro Ramalli <sup>2,3</sup>, Piero Tortoli <sup>3</sup>,  
Jianwen Luo <sup>1,\*</sup> and Jan D'hooge <sup>2,\*</sup>

<sup>1</sup> Center for Bio-Medical Imaging Research, Dept. of Biomedical Engineering, School of Medicine, Tsinghua University, Beijing 10084, China; tonglingpku@gmail.com (L.T.); cmuheqiong@163.com (Q.H.)

<sup>2</sup> Lab. On Cardiovascular Imaging and Dynamics, Dept. of Cardiovascular Sciences, KU Leuven, 3000 Leuven, Belgium; alejao16@gmail.com (A.O.); alessandro.ramalli@unifi.it (A.R.)

<sup>3</sup> Dept. of Information Engineering, University of Florence, 50139 Firenze, Italy; piero.tortoli@unifi.it

\* Correspondence: luo\_jianwen@tsinghua.edu.cn (J.L.); jan.dhooge@uzleuven.be (J.D.);  
Tel.: +86-10-6278-0650 (J.L.); +32-16-3-49012 (J.D.)

Received: 29 August 2018; Accepted: 26 January 2019; Published: 31 January 2019



**Abstract:** (1) Background: Multi-line transmit (MLT) beamforming has been proposed for fast cardiac ultrasound imaging. While crosstalk between MLT beams could induce artifacts, a Tukey ( $\alpha = 0.5$ )-Tukey ( $\alpha = 0.5$ ) transmit-receive (TT-) apodization can largely—but not completely—suppress this crosstalk. Coded excitation has been proposed for crosstalk suppression, but only for synthetic aperture imaging and multi-focal imaging on linear/convex arrays. The aim of this study was to investigate its (added) value to suppress crosstalk among simultaneously transmitted multi-directional focused beams on a phased array; (2) Methods: One set of two orthogonal Golay codes, as well as one set of two orthogonal chirps, were applied on a two, four, and 6MTL imaging schemes individually. These coded schemes were investigated without and with TT-apodization by both simulation and experiments; and (3) Results: For a 2MLT scheme, without apodization the crosstalk was removed completely using Golay codes, whereas it was only slightly suppressed by chirps. For coded 4MLT and 6MLT schemes, without apodization crosstalk appeared as that of non-apodized 2MLT and 3MLT schemes. TT-apodization was required to suppress the remaining crosstalk. Furthermore, the coded MLT schemes showed better SNR and penetration compared to that of the non-coded ones. (4) Conclusions: The added value of orthogonal coded excitation on MLT crosstalk suppression remains limited, although it could maintain a better SNR.

**Keywords:** multi-line transmit; crosstalk artifacts; coded excitation; cardiac imaging

## 1. Introduction

High frame rate imaging has recently gained increased attention in the field of echocardiography given its potential to reveal new areas of myocardial mechanics and blood flow analysis [1]. Among high frame rate imaging approaches, plane wave or diverging wave imaging are popular research topics due to their capacity to produce very high frame rates by scanning a given field-of-view (i.e., a 90-degree sector) with only a few transmissions [2–4]. However, the signal-to-noise ratio (SNR), spatial and contrast resolution of the resulting images are degraded due to the lack of focusing. To compensate this limitation, spatial coherent compounding is generally required in which the same region is interrogated several times from different directions and the final image is an average of all acquisitions [5]. As a drawback, the effective gain in frame rate drops by a factor equal to the number of the compounded images. Moreover, motion artifacts can often occur during compound.

Additionally, plane waves or diverging waves spread energy over a large area leading to small acoustic pressure amplitudes. Hence, it is technically challenging to make harmonic imaging.

As an alternative, multi-line transmit beamforming (MLT) has also been proposed [6,7]. In this approach, multiple focused beams are simultaneously transmitted into different directions leading to a gain in frame rate equal to the number of MLT beams. Typically, to simultaneously obtain multiple focused beams, the pulses that would be applied to individual elements to sequentially generate focused beams at different directions during several transmit events can be literally superimposed and be applied to those elements during a single transmit event. As an example, Figure 1 shows the pulses that would be used to generate four ultrasound beams either sequentially (Figure 1a–d) or simultaneously (i.e., 4-MLT) (Figure 1e). Figure 1f presents the transmit beam pattern corresponding to a case of 4MLT (Figure 1e). In contrast to plane wave/diverging wave imaging, MLT utilizes focused beams. This implies that the resulting SNR and spatial resolution [8,9] can be preserved as well as the possibility of a second harmonic imaging [10]. Despite these advantages, MLT beams may potentially introduce crosstalk that would appear as ghost-like artifacts on the images (Figure 2a). Intrinsically, crosstalk artifacts are the results of the interference between MLT beams in different directions. It has been demonstrated that such crosstalk artifacts can be largely suppressed by using a Tukey ( $\alpha = 0.5$ )-Tukey ( $\alpha = 0.5$ ) (TT) transmit and receive apodization scheme; so that the resulting MLT images look competitive to the conventional single line transmit beamforming (SLT) (Figure 2b) [8,9,11]. Nonetheless, despite these promising results, residual crosstalk artifacts can sometimes be detected [9]. Recently, alternative approaches, such as minimum variance (MV) receive beamforming [12], low complexity adaptive (LCA) receive apodization [13], and filtered delay multiply and sum (F-DMAS) [14] have been proposed to reduce receive crosstalk. Indeed, MV adaptive beamforming could not obtain the same crosstalk reduction as simply using a Tukey apodization when received, though a better spatial resolution could be obtained [12]. Similar, the LCA adaptive apodization method using a modified predefined apodization bank could have slightly better crosstalk reduction while improving the contrast and spatial resolution, but artifacts remained visible when hyperechoic structures were presented (for instance the pericardium) [13]. The F-DMAS method could provide a better receive crosstalk suppression but the contrast-to-noise ratio would be degraded [14]. Nonetheless, more attempts for better reduction of crosstalk remain desired.

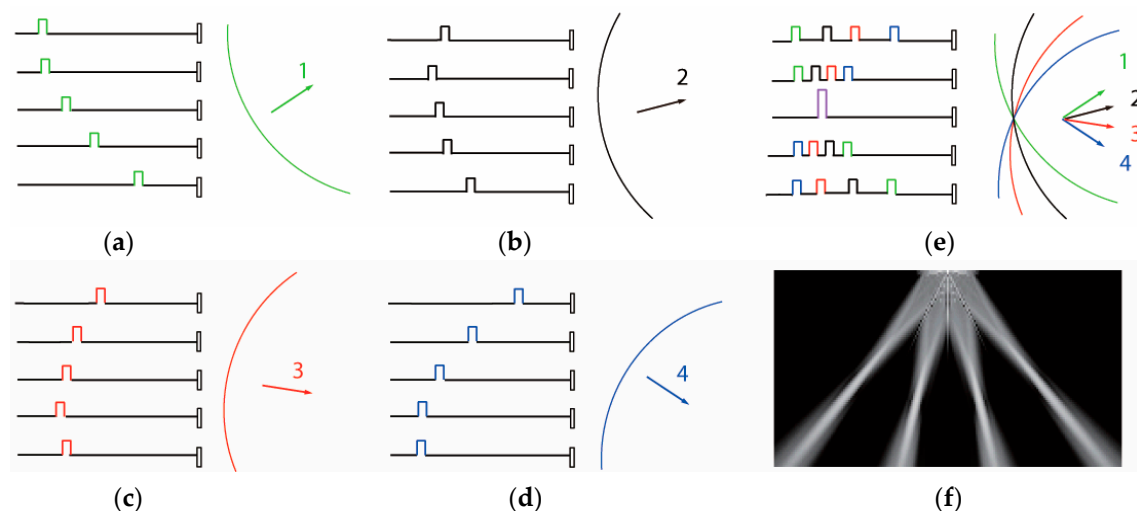


**Figure 1.** Pulses to be applied on individual elements of a phased array transducer in order to generate four focused transmit beams: (a) Transmit direction 1, (b) transmit direction 2, (c) transmit direction 3, (d) transmit direction 4, consecutively, or (e) simultaneously; and (f) A beam pattern of 4 simultaneously transmit beams.

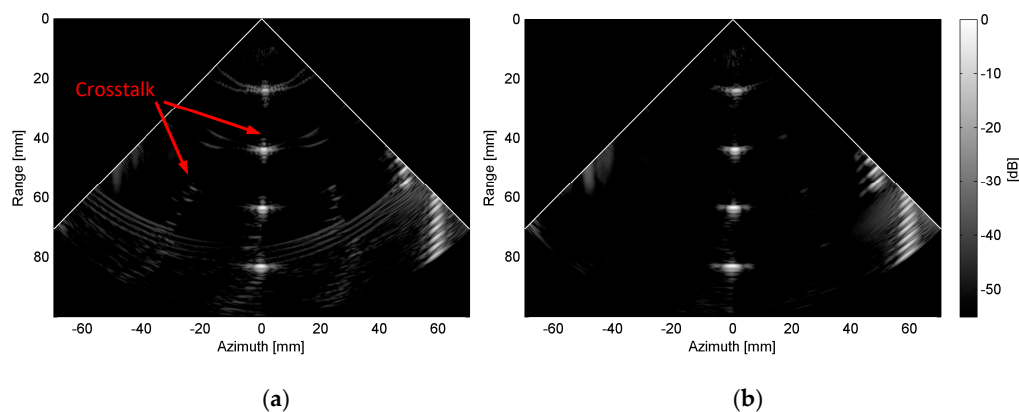


**Figure 2.** Reconstructed images of a wire phantom in water acquired using a 4-MLT (Multi-line transmit) imaging scheme (a) without apodization, the ghost-like crosstalk artifacts are presented; and (b) with a Tukey ( $\alpha = 0.5$ )-Tukey ( $\alpha = 0.5$ ) apodization on transmit and receive, the crosstalk artifacts are suppressed significantly.

Coded excitation has been shown to improve the penetration, signal-to-noise ratio, as well as the frame rate for ultrasound imaging. In terms of increasing frame rate, it has been proposed to suppress crosstalk in many applications [15–21] by using simultaneous transmission, of two or more orthogonal transmit pulses whose mutual cross-correlation is very small. When simultaneously transmitting two or more such mutually orthogonal codes, the received signals contain information from all codes. This information can then be separated through decoding process. Common orthogonal codes are the Golay or chirp codes. Golay codes possess a good orthogonal property, but require the transmission of complementary code pairs to constrain the range lobes, which in turn halve the effective frame rate. On the other hand, orthogonal chirp pairs can be obtained by sweeping a certain frequency band in opposite directions or by sweeping separate frequency (sub)bands. For the former case, the cross-correlation of two orthogonal chirps can be relatively high, whereas the imaging performance of the latter is typically limited by the narrow bandwidth of ultrasound transducers. However, for chirps, the transmission of complementary codes is not necessary, and so the frame rate would be compromised. Both orthogonal Golay and chirp codes have been proposed for crosstalk reduction in increasing frame rate for synthetic aperture imaging with multiple transmit positions [15,17] and in maintaining frame rate for multi-zone focusing by simultaneous transmissions for linear [16–19,22] and convex array imaging [20,21]. However, towards phased array based high frame rate cardiac imaging, it has not been revealed yet that the feasibility of using these orthogonal codes to (further) reduce crosstalk among focused MLT beams. Hence, the aim of this study was to test this feasibility in both simulation and experimental setups.

## 2. Materials and Methods

In this study, a typical 1-D cardiac phased array probe (PA230, Esaote SpA, Florence, Italy) with 128 elements, a central frequency of 2.0 MHz and a bandwidth of 50% was used both for simulation and experiments. The array measured 21.6 mm in width and 13 mm in height with a pitch of 170  $\mu\text{m}$ . To accommodate our experimental system, which possesses 64 independent channels, only the odd elements were pinned, resulting in an equivalent 64-element phased array with an effective pitch of 340  $\mu\text{m}$ . This choice was made so as to exploit the maximum aperture of the probe (22 mm) with the 64 available channels on the system; the selection of 64 consecutive elements would have reduced the aperture size to 11 mm, thus limiting the lateral resolution that is already poor in cardiac phased array imaging. Moreover, for a central frequency of 2.0 MHz, the corresponding central wavelength of the probe is 770  $\mu\text{m}$  at a speed of sound of 1540 cm/s. Thus, the effective pitch of 340  $\mu\text{m}$  is about half of the central wavelength. This limits the possibility to produce grating lobes when steering the beams out at 45 degrees, i.e., the typical maximum steering angle in cardiac imaging.

## 2.1. Orthogonal Coded Excitations

On this probe, two types of orthogonal coded excitations, i.e., one set of orthogonal Golay codes and one set of orthogonal linear frequency (FM) modulated chirps were tested since they have already been proposed for other purposes in ultrasound imaging [12–19] and are relatively simple to implement. In particular, the following Golay codes were used to obtain good orthogonal property without largely elongating the excitation duration:

$$G1: [1, 1, 1, -1]; G1c: [1, 1, -1, 1]; G2: [1, -1, 1, 1]; \text{ and } G2c: [1, -1, -1, -1].$$

where  $G1$  is complementary to  $G1c$ ,  $G2$  is complementary to  $G2c$ , the pair of  $G1$  and  $G1c$  are orthogonal to the pair of  $G2$  and  $G2c$ . The excitations were obtained by convolving every Golay codes with a burst of 1.45 cycles square wave at the central frequency of the transducer, respectively, that resulted in a duration of 2.91  $\mu\text{s}$ .

A linear FM chirp coded excitation can be defined as:

$$c(t) = a(t) \cdot \exp \left[ j2\pi \left( f_0 t + \frac{B}{2T} t^2 \right) \right], \quad -\frac{T}{2} \leq t \leq \frac{T}{2}, \quad (1)$$

where  $a(t)$  is the tapering function,  $f_0$  is the central frequency,  $B$  is the bandwidth of the chirp signal, and  $T$  is the signal duration. In our case to have better orthogonality,  $a(t)$  was a Tukey window ( $\alpha = 0.2$ ),  $T$  was 10  $\mu\text{s}$ , and  $B$  was 3.8 MHz centered around 2 MHz. Two orthogonal chirps,  $c_{up}$  and  $c_{down}$ , were obtained by sweeping  $B$  with the opposite directions. The different excitation signals are sketched in Figure 3. Note that the large sweeping bandwidth of the chips codes were chosen to minimize the Fresnel ripples around the pass-band of the probe for a better response, as indicated in Figure 4. Moreover, to decode, matched filters were used for the Golay codes, whereas Chebyshev-apodized mis-matched filters were adopted for the chirps.

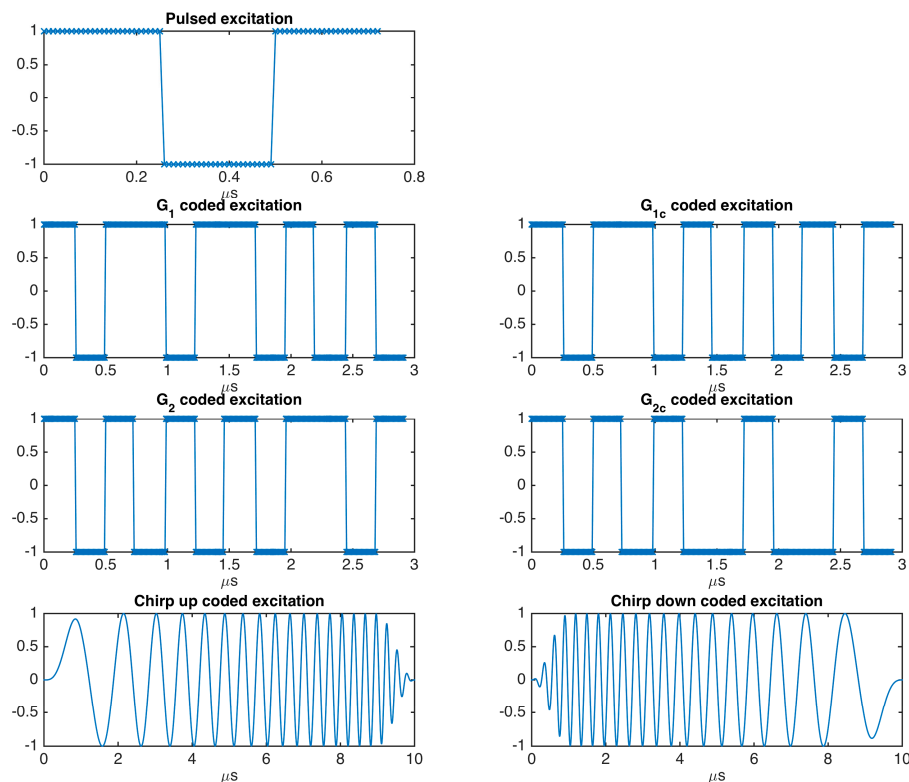
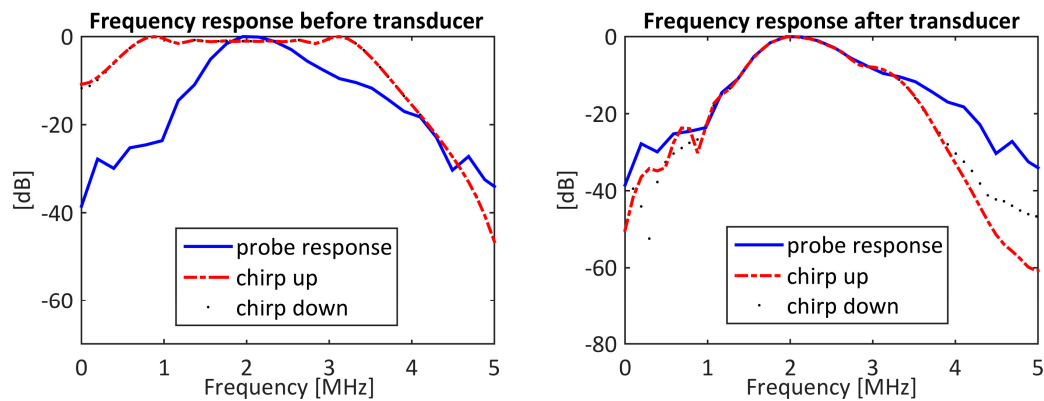


Figure 3. Plots of different excitation signals.





**Figure 4.** Frequency response of the two chirp codes.

## 2.2. Coded Excitation Based Multi-Line Transmit (MLT) Imaging Schemes

Using the two sets of orthogonal codes, a 2, 4, and 6-MLT imaging scheme were set up. The MLT transmits were obtained by superimposing the transmit pulse patterns that would be applied to the probe elements to generate subsequent transmit beams [8]. The imaging sector was set to  $90^\circ$  and covered by 180 image lines. For a given MLT imaging scheme, an orthogonal code pair was applied on neighboring MLT beams in an interleaved manner, as illustrated in Figure 5, i.e., neighboring sub-sectors were scanned using MLT beams with orthogonal codes. In this way, signals generated from neighboring MLT beams were expected to be better differentiated through decoding in reception, which was performed before beamforming.

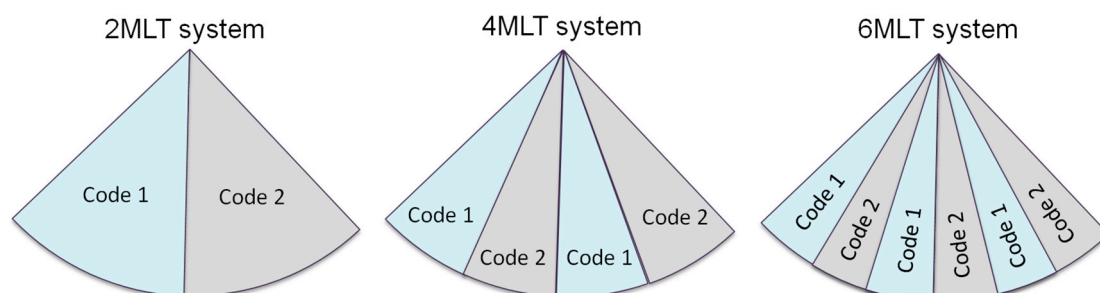


**Figure 5.** Illustration of the interleaving arrangement of two orthogonal codes on a given MLT imaging scheme. Code 1 and code 2 are mutual orthogonal codes.

## 2.3. Simulations

The performance of coded excitation imaging scheme was first investigated *in silico* through the simulation software Field II [23,24] based on the phased array described at the beginning of this section. To benchmark, an SLT imaging scheme, 2, 4, and 6-MLT schemes using a burst excitation (1.45 cycles square wave at 2 MHz) were included. For all imaging schemes, the transmit focal point was maintained at a depth of 70 mm and a dynamic apodization with  $f\#$  of two was adopted in reception. As previously proposed, a Tukey ( $\alpha = 0.5$ )–Tukey ( $\alpha = 0.5$ ) (TT) apodization scheme on transmit and receive were also tested on different MLT schemes (coded and non-coded) for crosstalk suppression [8,9].

To appreciate the spatial resolution as well as the crosstalk artifacts, the point-spread-functions (PSFs) of different imaging schemes were simulated. In particular, four point scatterers were positioned at depths from 30 mm to 90 mm with an equal axial interval of 20 mm. In the azimuth direction, they were positioned at 10 mm offset of the transducer symmetry axis to better appreciate the potential crosstalk. A given PSF profile was evaluated by the  $-6$  dB beam width in both radial and lateral directions. The crosstalk was quantified by calculating the intensity difference between the PSF of a

given MLT scheme and that of the SLT imaging scheme ( $xtalk_{psf}$ ). For details on the definitions of these parameters, please refer to Formulas (3), (5), and (7) in Reference [9].

#### 2.4. Experimental Validation

To experimentally investigate the performance of the coded MLT schemes, the imaging schemes defined in Section 2.3 were implemented on the ultrasound advanced open platform (ULA-OP) [25,26] equipped with the above mentioned phased array transducer. The pulse repetition frequency (PRF) was 4750 Hz and the prebeamformed radio-frequency (RF) channel data were acquired at a sampling frequency of 50 MHz using the ULA-OP acquisition board [27] and beamformed offline through MATLAB R2015a (The MathWorks, Natick, MA, USA). The beamforming parameters were the same as those applied in the simulations.

Using these setups, a general-purpose tissue mimicking phantom (CIRS Model 040GSE, Norfolk, VA, USA) and the left ventricle of a healthy volunteer from a parasternal long axis view were imaged. To quantify the image quality, the contrast-to-noise (CNR), the contrast ratio (CR) of the cystic regions, and the signal-to-noise ratio (SNR) were calculated for the static phantom images:

$$CNR = \frac{\mu_b - \mu_c}{\sqrt{\sigma_b^2 + \sigma_c^2}}, \quad (2)$$

$$CR = 20 \log_{10} \frac{\mu_b}{\mu_c} \quad (3)$$

$$SNR = 10 \log_{10} \frac{\mu_b}{\mu_n} \quad (4)$$

where  $\mu_b$  and  $\mu_c$ ,  $\mu_n$ , are the mean gray-level in the background, the cystic regions and in the noise region, respectively, and  $\sigma_b$  and  $\sigma_c$  are their corresponding standard deviations. Finally, the quality of the in-vivo images was visually examined.

### 3. Results

The simulated PSFs of different MLT schemes without and with coded excitation are presented in Figures 6–8. Without apodization on transmit and receive, no crosstalk was seen in the image of the Golay-coded 2-MLT scheme (Figure 6c) within a 55 dB-dynamic range, whereas a slight crosstalk suppression was observed in the image of the chirp-coded 2-MLT scheme (Figure 6d, highest crosstalk at about −46 dB) compared to that of the non-coded 2-MLT scheme (Figure 6b, highest crosstalk at about −40 dB). For the non-apodized coded 4-MLT and 6-MLT schemes, obvious crosstalk artifacts was observed (Figure 7c–f), though less artifacts were found on the Golay-coded images than on the chirp-coded images in particular in the near field. With TT apodization, most of the crosstalk was suppressed within the 55 dB-dynamic range (Figure 8), despite the fact that the image of the point scatterer at the depth of 30 mm was severely distorted for the TT-apodized chirp-coded 6MLT scheme. Quantitative crosstalk evaluation is shown in Figure 9. It was found that, without apodization and for the same number of MLT beams, Golay-coded MLT schemes presented the lowest crosstalk level. In particular, zero level crosstalk was detected for Golay-coded 2-MLT schemes. Moreover, with apodization, the crosstalk level of both Golay and chirp-coded 4MLT and 6MLT schemes was significantly reduced compared to that of the non-apodized ones. In general, despite of the apodized chirp-coded 6MLT schemes, all apodized coded MLT schemes showed lower crosstalk compared to the corresponding non-apodized non-coded MLT schemes.

In addition, for the mean radial beam widths, all imaging schemes showed similar values (around 1mm), although Golay-coded schemes had slightly larger values (about 1.07 mm) (Figure 10, top plot). With respect to lateral beam widths, the non-apodized coded schemes showed similar widths, which was about 2.30 mm, whereas the values of apodized schemes were around 2.89 mm (Figure 10, bottom plot).

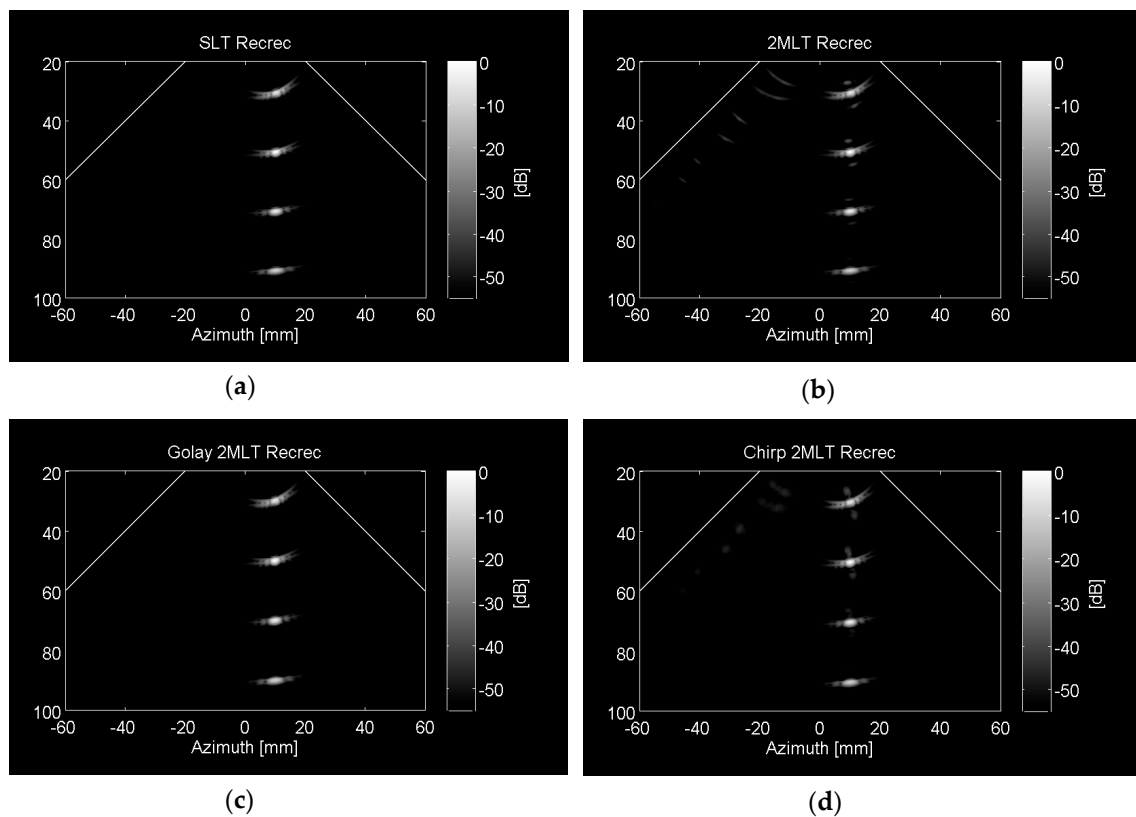


**Figure 6.** Point-spread-function (PSF) of different MLT schemes without apodization on transmit and receive. (a) SLT (single line transmit i.e., 1MLT) scheme with non-coded excitation as the reference image, (b) 2MLT scheme using non-coded excitation with crosstalk artifacts, (c) 2MLT scheme using Golay coded excitation without crosstalk artifacts, and (d) 2MLT scheme using chirp coded excitation with slight crosstalk artifacts. A dynamic range of 55 dB was used.

Based on the simulation results, TT-apodized 4MLT and 6MLT schemes were tested in in-vitro experiments. Results are presented in Figures 11 and 12 where in Figure 12 the cystic regions were zoomed for better visualization. The images of the tissue phantom presented in Figure 11 showed that the crosstalk artifacts were hardly observed for all MLT schemes. However, the coded images showed better contrast for both the middle and bottom cystic regions (Figure 12). Moreover, coded images presented less electronic background noise compared to the non-coded ones (Figure 11, indicated by the arrows). Quantitatively, seven regions of interest (ROI) were defined on those images to compute the SNR, CNR, and CR. As indicated in Figure 11a, three ROIs were defined in the three cystic regions by adjusting the radius of the cysts, whereas three ROIs were accordingly defined in the hyperechoic background next to individual cysts. The CNR and CR of each cystic region were thus computed using Equations (2) and (3). Moreover, the last ROI was defined in the noise region (Figure 11,  $N_{ROI}$ ), where the SNR was computed based on signal in  $N_{ROI}$  and  $B_{ROI}$  using Equation (4). The results are presented in Table 1. It can be seen that in terms of CNR, all MLT imaging schemes showed similar values for the top and middle cysts, whereas for the bottom cyst, the coded 4-MLT and 6-MLT schemes showed higher values than that of the non-coded 4-MLT and 6-MLT schemes, respectively. In terms of CR, except for the top cyst, coded schemes showed about 2.1–5.5 dB higher CR compared to that of the non-coded ones; the chirp-coded MLT schemes presented the highest CR values. Similarly, with respect to SNR, the coded schemes had about 2.6–5.4 dB higher SNR than that of the non-coded ones; still, the Golay-coded performed the best and presented the highest SNR.

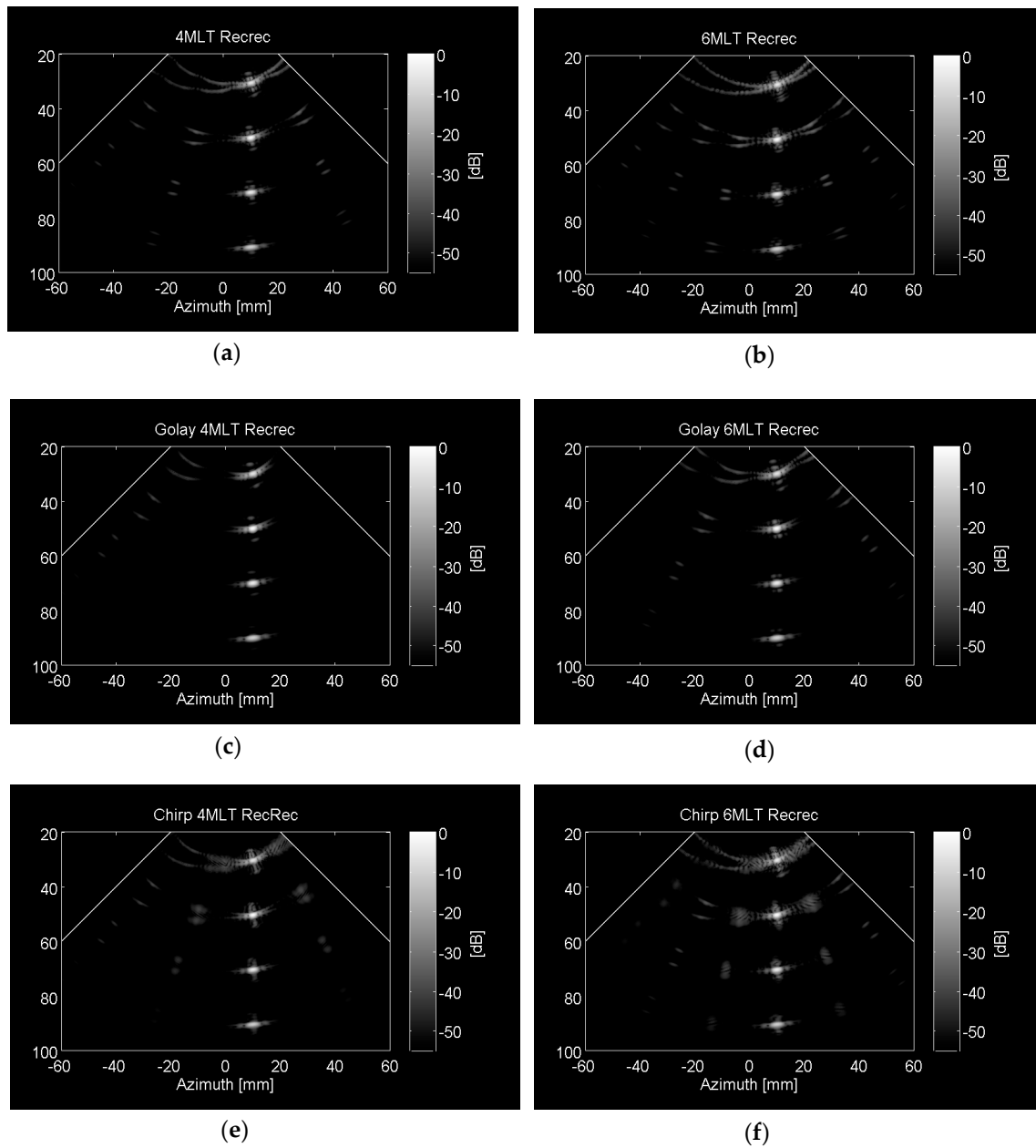


**Figure 7.** Point-spread-function (PSF) of 4MLT and 6MLT schemes using (a,b) non-coded excitation; (c,d) Golay coded excitations; and (e,f) chirp coded excitations. No apodization was applied on transmit and receive. Crosstalk artifacts appeared and became more severe as increasing the MLT beams.

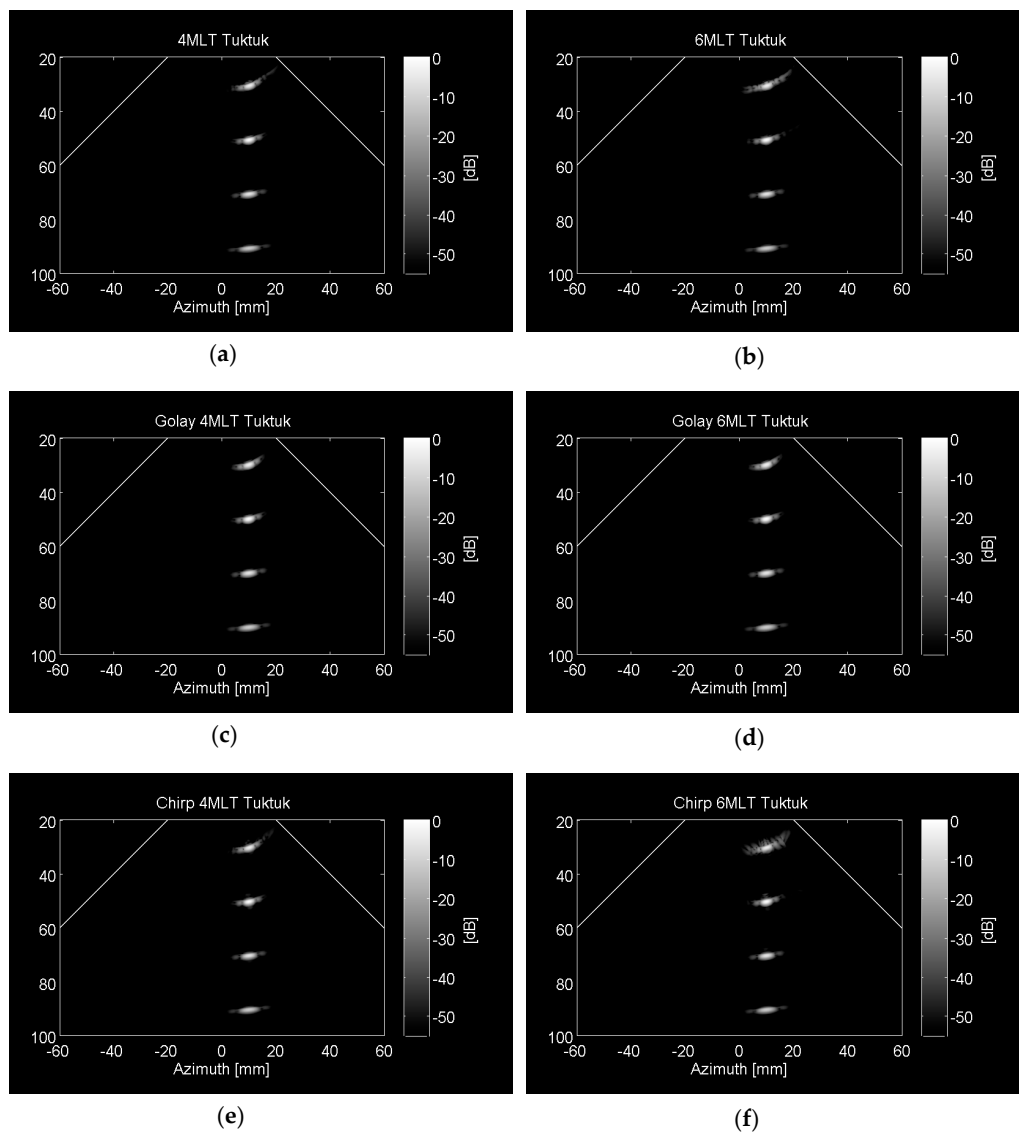


**Figure 8.** Point-spread-function (PSF) of 4MLT and 6MLT schemes using (a,b) non-coded excitation; (c,d) Golay coded excitations; and (e,f) chirp coded excitations. Tukey ( $\alpha = 0.5$ )-Tukey ( $\alpha = 0.5$ ) apodization scheme was applied on transmit and receive that the crosstalk artifacts were largely suppressed.

**Table 1.** Quantifications of different Tukey-Tukey apodized multi-line transmit (MLT) schemes.

Imaging Schemes	Non-Coded 4-MLT	Non-Coded 6-MLT	Golay-Coded 4-MLT	Golay-Coded 6-MLT	Chirp-Coded 4-MLT	Chirp-Coded 6-MLT
CNR <sub>top</sub>	1.28	1.31	1.18	1.15	1.24	1.28
CNR <sub>middle</sub>	1.53	1.40	1.49	1.50	1.56	1.60
CNR <sub>bottom</sub>	1.82	1.01	2.05	1.31	2.25	1.51
CR <sub>top</sub> (dB)	9.54	10.75	8.11	9.40	9.93	10.50
CR <sub>middle</sub> (dB)	17.26	14.49	20.40	17.76	19.41	20.01
CR <sub>bottom</sub> (dB)	11.55	6.50	14.52	8.12	16.03	9.99
SNR (dB)	12.71	10.66	18.15	16.17	15.94	13.31
Frame rate (Hz)	105.56	158.33	52.78	79.17	105.56	158.33

Finally, in-vivo images of a healthy volunteer were acquired with the three TT-apodized 4MLT schemes (Figure 13). From the cine-loops (Supplementary Materials: Video S1: Figure13\_a; Video S2: Figure13\_b; Video S3: Figure13\_c), the coded images seemed to have better contrast between the myocardial and blood pool and no obvious crosstalk was observed.

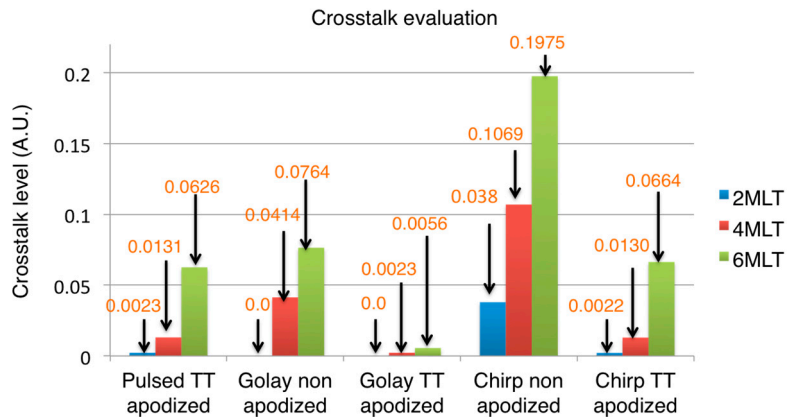


**Figure 9.** Crosstalk evaluation of different MLT schemes. TT: Tukey ( $\alpha = 0.5$ )-Tukey ( $\alpha = 0.5$ ) apodization scheme.

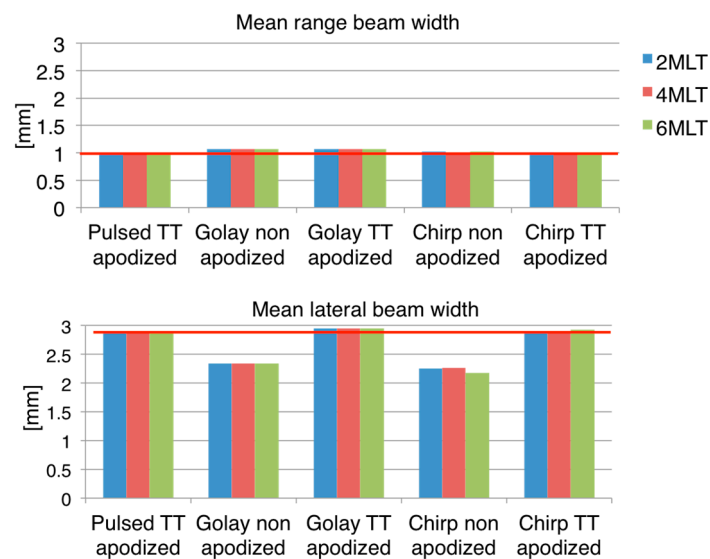


**Figure 10.** Beam widths in radial (upper panel) and lateral (lower panel) directions estimated from the point-spread-function (PSF). The red line indicates the value of a non-coded SLT scheme using TT apodization. TT: Tukey ( $\alpha = 0.5$ )-Tukey ( $\alpha = 0.5$ ) apodization scheme.



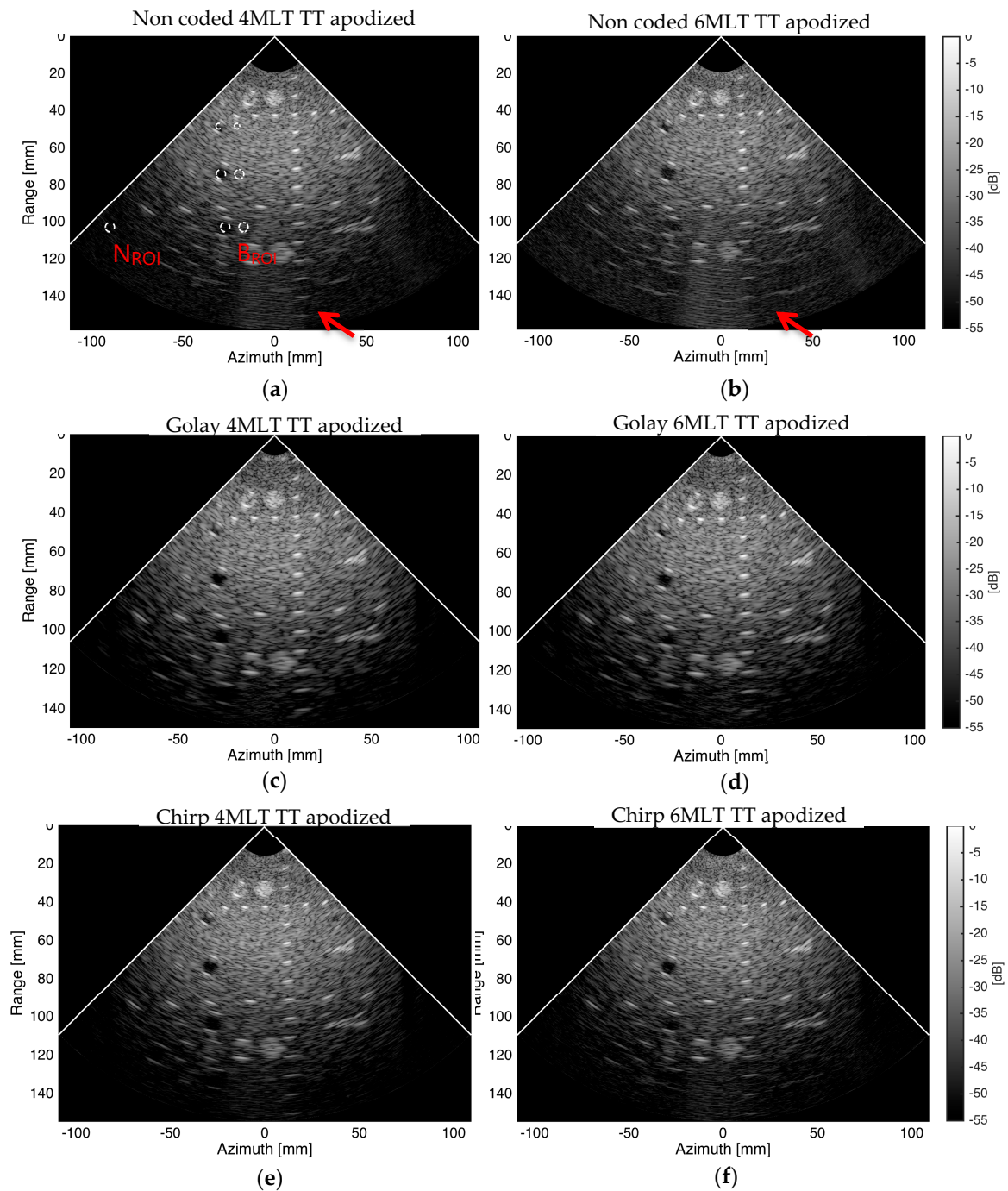


**Figure 11.** Tissue phantom images of the 4MLT and 6MLT schemes using (a,b) non-coded; (c,d) Golay-coded excitation; or (e,f) chirp-coded excitation. TT apodization was applied on both transmit and receive. TT: Tukey ( $\alpha = 0.5$ )-Tukey ( $\alpha = 0.5$ ) apodization scheme. A dynamic range of 55 dB was used. The arrows in panel (a) and (b) point the areas in which the non-coded MLT schemes started to lose signal-to-noise ratio (SNR).

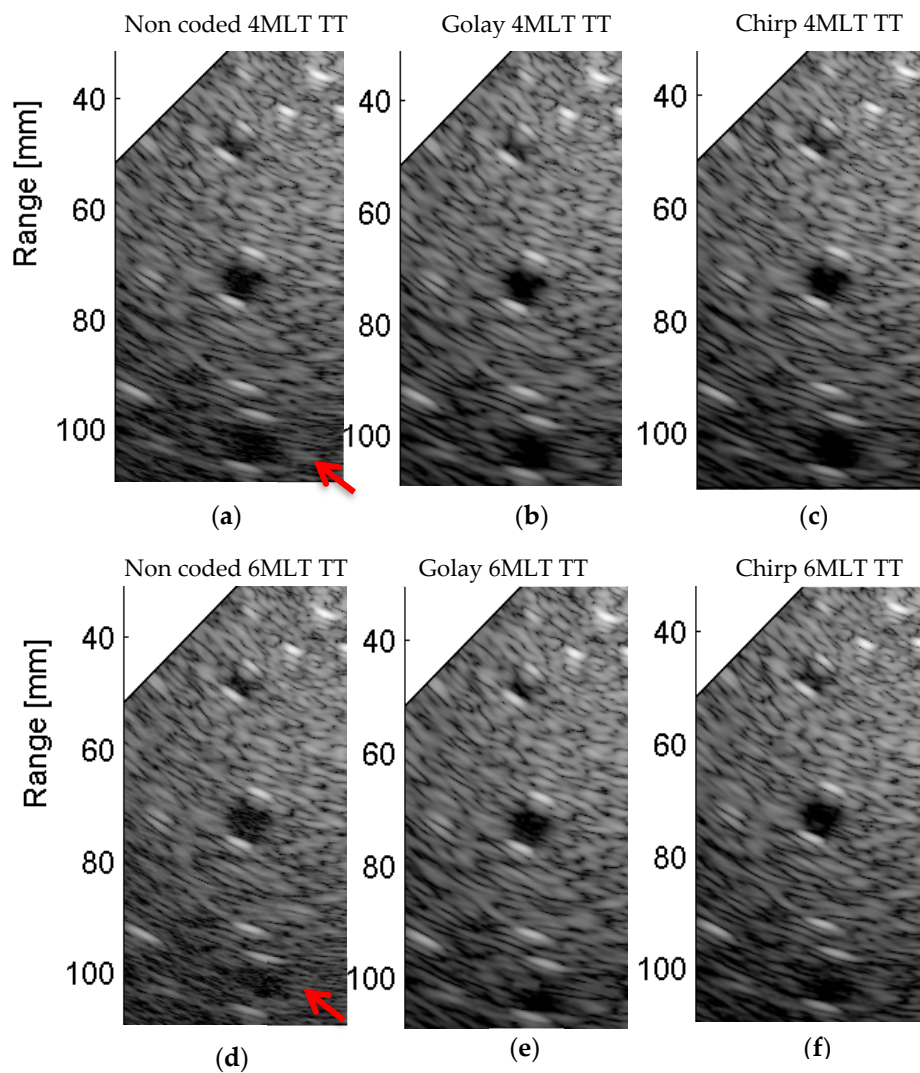


**Figure 12.** Zoomed in tissue phantom images of the 4MLT and 6MLT schemes using (a,d) non-coded; (b,e) Golay-coded excitation; or (c,f) chirp-coded excitation. TT apodization was applied on both transmit and receive. TT: Tukey ( $\alpha = 0.5$ )-Tukey ( $\alpha = 0.5$ ) apodization scheme. A dynamic range of 55 dB was used. The arrows in panel (a) and (d) point the areas in which the non-coded MLT schemes started to lose SNR.

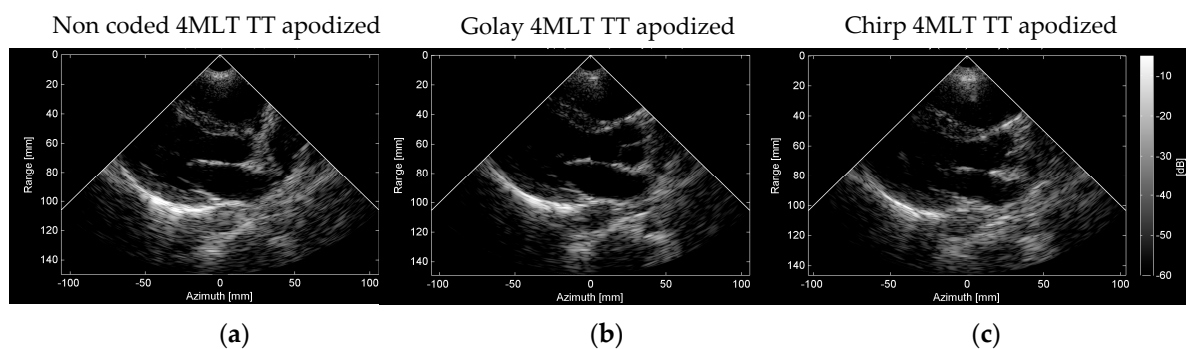


**Figure 13.** In-vivo examples of 4MLT schemes using (a) non-coded excitation, (b) Golay coded excitation, and (c) chirp coded excitation with TT apodization. TT: Tukey ( $\alpha = 0.5$ )-Tukey ( $\alpha = 0.5$ ) apodization scheme. Video clips available online. A dynamic range of 55 dB was used (video clips available as Supplementary Materials).

#### 4. Discussion

In this study, we investigated the impact of two types of orthogonal codes on phased array based MLT imaging schemes in order to see whether they could be of (added) value to suppress the associated crosstalk artifacts. The performance of these coded imaging schemes was investigated without and with TT apodization and benchmarked against non-coded MLT schemes with TT apodization in both simulation and experiments. The results show that without apodization, for a 2MLT scheme, the crosstalk was completely removed using orthogonal Golay codes with a 55 dB dynamic range, whereas it was slightly suppressed with the orthogonal chirps (Figures 6 and 9). Indeed, this implied extremely low cross-correlation between the used orthogonal Golay pair. Compared to a non-coded non-apodized four or 6-MLT scheme, a coded non-apodized four or 6-MLT scheme showed less crosstalk artifacts and the appearance of its artifacts largely replicated that of a non-coded non-apodized two or 3-MLT scheme, respectively (Figure 7). This was to be expected given that only two sets of orthogonal codes were applied on neighboring MLT beams in an interleaved manner. Hence, to suppress the remaining crosstalk, TT apodization was applied (Figure 8). While almost no crosstalk artifacts could have been seen on the TT-apodized coded images (Figure 8), crosstalk quantification showed that the chirp-coded schemes had slightly higher crosstalk level than that of the Golay-coded ones (Figure 9). This was in agreement with the fact that the cross-correlation of the two “orthogonal” chirps remained high due to the overlapping sweeping frequency bands. The information in two different directions can thus not be completely separated. Moreover, in the near field, the PSF of the chirp-coded 6MLT scheme distorted [e.g., Figure 8f the scatterer at a depth of 30 mm]. This might be due to the fact that the inter-beam space was very small for the 6MLT scheme when it was close to the probe, since the duration of the chirps were relatively long, the level of interference between simultaneously transmitted waveforms could be too high to be well separated in the near field. Nonetheless, with respect to crosstalk artifacts, experimental images of the apodized coded MLT schemes showed similar quality compared to that the non-coded schemes (Figures 8 and 11–13). It is important to note that the effective gain in frame rate of the Golay-coded schemes was compromised by a factor of two due to the transmission of complementary codes (Table 1).

Concerning spatial resolution, the coded schemes had slightly worse axial resolution whereas the lateral resolution was almost not affected (Figure 10); the latter, as is known, is affected by TT apodization. Moreover, as expected, the coded schemes had significantly improved the penetration, SNR, and contrast, especially at larger depths (Figures 11 and 12, Table 1). This was also expected given that more energy was transmitted into the tissue with the coded schemes given the increased time-bandwidth product [28]. It should be noticed that the transmit power of different imaging schemes was not normalized in order to make the different imaging schemes operating at their individual optimal conditions. Furthermore, the different blind regions of the experimental images are due to different signal lengths; indeed, longer excitations keep the transmitters switched on for longer times, during which the receivers are disabled.

Regarding crosstalk reduction, the tested Golay and chirp codes did not show much added value, and indeed, the apodization is still mandatory; the number of MLT beams is usually larger than the number of the orthogonal codes, hence the cross-talk cannot be perfectly suppressed; the frame rate might be decreased by a factor of two when complementary codes are needed. On the other hand, coded signals are beneficial in terms of SNR and penetration depth that are limited by MLT transmission schemes. In the latter, the pulse patterns transmitted to generate simultaneous beams, are given by the superimposition of different signals [7]. This superimposition leads to fully constructive interferences on the central elements. As such, the amplitudes applied on non-central elements would decrease since the maximal peak-peak voltage level is fixed on a given system, force a decrease of the amplitudes on the non-centered elements. As a consequence, less energy is transmitted, which would lower the penetration and SNR. The more the MLT beams, the lower the transmitted energy on a given MLT beam. This effect was well demonstrated in Figure 11a,b. In this perspective, coded excitation could thus be an alternative in maintaining the transmit energy/penetration in MLT imaging,

particularly for schemes with a larger number of MLT beams. Moreover, a TT-apodized Golay-coded 4-MLT, 6-MLT, and a chirp-apodized 4-MLT could be good candidates as imaging scheme providing a good tradeoff between frame rate and signal-to-noise ratio. As a preliminary test, only one set of in-vivo images using Golay-coded 4-MLT and Chirp coded 4-MLT schemes were acquired. Further in-vivo investigation is the topic of the on-going work.

Finally, it should be noted that for either Golay or chirp codes, only two sets of orthogonal coded excitations were adopted since finding larger number of mutually orthogonal codes was challenging. Indeed, to have more mutually orthogonal Golay codes, the excitation duration would be significantly increased and/or more sets of complementary codes would be required [29,30]. Long excitation duration could lead to a large dead zone and strong interference of the MLT beams in the near field, whereas sending more complementary codes would result in no benefit in frame rate. As for chirp codes, more mutually orthogonal codes could be obtained by subdividing the transducer pass-band and by increasing the code duration. However, the transducer pass-band would not be effectively used, thus limiting the achievable range resolution. Moreover, a larger dead zone could appear close to the transducer surface as well as more near-field artifacts due to higher interference between MLT beams with longer codes. Finally, stitching artifacts were seen in the in-vivo images as previously demonstrated in [9]. However, in the present study, this was not compensated, as described in Reference [31], since the primary purpose was to investigate the capability of coded excitation on crosstalk suppression.

## 5. Conclusions

The main goal of this study was to investigate the impact of orthogonal coded excitation for MLT crosstalk suppression. The results demonstrated that coded excitation could be used to suppress MLT crosstalk, although a Tukey-Tukey apodization is still required when the number of MLT beams is larger than the number of orthogonal codes. Moreover, coded excitation could help maintain the transmit energy (thus the SNR), which can be largely reduced as a result of increasing MLT beams. Overall, the benefit of applying coded excitation on an MLT imaging scheme to further suppress crosstalk artifacts remains limited, however when seeking a balance between frame rate and SNR, coded excitation could indeed be a valid alternative.

**Supplementary Materials:** The following are available <http://www.mdpi.com/2076-3417/9/3/486/s1>, Video S1: Figure13\_a; Video S2: Figure13\_b; Video S3: Figure13\_c.

**Author Contributions:** Conceptualization, L.T., A.O., J.D.; Methodology, L.T., A.O.; Software, L.T.; Validation, L.T., Q.H., and A.R.; Writing-Original Draft Preparation, L.T.; Writing-Review & Editing, L.T., J.D., P.T., A.R., J.L., Q.H.; Visualization, L.T.; Supervision, J.D., J.L., P.T.; Funding Acquisition, L.T., A.R., J.L., J.D. and P.T.

**Funding:** The research leading to these results has received funding from China Postdoctoral Science Foundation (2014M560094), National Natural Science Foundation of China (81471665, 61871251, and 81561168023), the National Key R&D Program of China (2016YFC0102200 and 2016YFC0104700), European Research Council under the European Union's Seventh Framework Programme (FP7/2007-2013)/ERC Grant Agreement number 281748. A. Ramalli is supported by the European Union's Horizon 2020 research and innovation programme under the Marie Skłodowska-Curie grant agreement No 786027 (ACOUSTIC).

**Conflicts of Interest:** The authors declare no conflict of interest.

## References

1. Cikes, M.; Tong, L.; Sutherland, G.R.; D'hooge, J. Ultrafast Cardiac Ultrasound Imaging. *JACC Cardiovasc. Imaging* **2014**, *7*, 812–823. [CrossRef] [PubMed]
2. Hasegawa, H.; Kanai, H. High-frame-rate echocardiography using diverging transmit beams and parallel receive beamforming. *J. Med. Ultrason.* **2011**, *38*, 129–140. [CrossRef]
3. Papadacci, C.; Pernot, M.; Couade, M.; Fink, M.; Tanter, M. High-contrast ultrafast imaging of the heart. *IEEE Trans. Ultrason. Ferroelectr. Freq. Control* **2014**, *61*, 288–301. [CrossRef] [PubMed]



4. Moore, C.; Castellucci, J.; Andersen, M.V.; Lefevre, M.; Arges, K.; Kisslo, J.; Von Ramm, O.T. Live high-frame-rate echocardiography. *IEEE Trans. Ultrason. Ferroelectr. Freq. Control* **2015**, *62*, 1779–1787. [[CrossRef](#)] [[PubMed](#)]
5. Montaldo, G.; Tanter, M.; Bercoff, J.; Benech, N.; Fink, M. Coherent plane-wave compounding for very high frame rate ultrasonography and transient elastography. *IEEE Trans. Ultrason. Ferroelectr. Freq. Control* **2009**, *56*, 489–506. [[CrossRef](#)] [[PubMed](#)]
6. Shirasaka, T. Ultrasonic imaging apparatus. U.S. Patent US4815043, 1989.
7. Mallart, R.; France, L.C.; Fink, M. Improved imaging rate through simultaneous transmission of several ultrasound beams. *SPIE* **1992**, *1733*, 120–130.
8. Tong, L.; Gao, H.; D’Hooge, J. Multi-transmit beam forming for fast cardiac imaging—a simulation study. *IEEE Trans. Ultrason. Ferroelectr. Freq. Control* **2013**, *60*, 1719–1731. [[CrossRef](#)]
9. Tong, L.; Ramalli, A.; Jasaityte, R.; Tortoli, P.; D’hooge, J. Multi-Transmit Beam Forming for Fast Cardiac Imaging—Experimental Validation and In Vivo Application. *IEEE Trans. Med. Imaging* **2014**, *33*, 1205–1219. [[CrossRef](#)]
10. Prieur, F.; Dénarié, B.; Austeng, A.; Torp, H. Multi-line transmission in medical imaging using the second-harmonic signal. *IEEE Trans. Ultrason. Ferroelectr. Freq. Control* **2013**, *60*, 2682–2692. [[CrossRef](#)]
11. Ramalli, A.; Dallai, A.; Guidi, F.; Bassi, L.; Boni, E.; Tong, L.; Fradella, G.; D’Hooge, J.; Tortoli, P. Real-Time High-Frame-Rate Cardiac B-Mode and Tissue Doppler Imaging Based on Multiline Transmission and Multiline Acquisition. *IEEE Trans. Ultrason. Ferroelectr. Freq. Control* **2018**, *65*, 2030–2041. [[CrossRef](#)]
12. Rabinovich, A.; Feuer, A.; Friedman, Z. Multi-line transmission combined with minimum variance beamforming in medical ultrasound imaging. *IEEE Trans. Ultrason. Ferroelectr. Freq. Control* **2015**, *62*, 814–827. [[CrossRef](#)] [[PubMed](#)]
13. Zurakhov, G.; Tong, L.; Ramalli, A.; Tortoli, P.; D’hooge, J.; Friedman, Z.; Adam, D. Multiline Transmit Beamforming Combined With Adaptive Apodization. *IEEE Trans. Ultrason. Ferroelectr. Freq. Control* **2018**, *65*, 535–545. [[CrossRef](#)] [[PubMed](#)]
14. Matrone, G.; Ramalli, A.; Savoia, A.S.; Tortoli, P.; Magenes, G. High Frame-Rate, High Resolution Ultrasound Imaging with Multi-Line Transmission and Filtered-Delay Multiply and Sum Beamforming. *IEEE Trans. Med. Imaging* **2016**, *PP*, 1–10. [[CrossRef](#)] [[PubMed](#)]
15. Chiao, R.Y.; Thomas, L.J. Synthetic transmit aperture imaging using orthogonal Golay coded excitation. In Proceedings of the 2000 IEEE Ultrasonics Symposium. Proceedings. An International Symposium, San Juan, Puerto Rico, 22–25 October 2000; pp. 1677–1680. [[CrossRef](#)]
16. Jeong, Y.K.; Song, T.-K. Simultaneous Multizone Focusing Method with Orthogonal Chirp Signals. In Proceedings of the IEEE Symposium on Ultrasonics, Atlanta, GA, USA, 7–10 October 2001; pp. 1517–1520.
17. Misaridis, T.; Jensen, J.A. Use of modulated excitation signals in medical ultrasound. Part III: High frame rate imaging. *IEEE Trans. Ultrason. Ferroelectr. Freq. Control* **2005**, *52*, 208–219. [[CrossRef](#)] [[PubMed](#)]
18. Chiao, R.Y.; Hao, X. Coded excitation for diagnostic ultrasound: A system developer’s perspective. *IEEE Trans. Ultrason. Ferroelectr. Freq. Control* **2005**, *52*, 160–170. [[CrossRef](#)] [[PubMed](#)]
19. Kim, B.H.; Kim, G.D.; Song, T.K. A post-compression based ultrasound imaging technique for simultaneous transmit multi-zone focusing. *Ultrasonics* **2007**, *46*, 148–154. [[CrossRef](#)] [[PubMed](#)]
20. Yoon, C.; Yoo, Y.; Song, T.-K.; Chang, J.H. Orthogonal quadratic chirp signals for simultaneous multi-zone focusing in medical ultrasound imaging. *IEEE Trans. Ultrason. Ferroelectr. Freq. Control* **2012**, *59*, 1061–1069. [[CrossRef](#)]
21. Yoon, C.; Lee, W.; Chang, J.; Song, T.K.; Yoo, Y. An efficient pulse compression method of chirp-coded excitation in medical ultrasound imaging. *IEEE Trans. Ultrason. Ferroelectr. Freq. Control* **2013**, *60*, 2225–2229. [[CrossRef](#)]
22. Kim, B.-H.; Song, T.-K. Multiple transmit focusing using modified orthogonal Golay codes for small scale systems. In Proceedings of the IEEE Symposium on Ultrasonics, Honolulu, HI, USA, 5–8 October 2003; pp. 1574–1577. [[CrossRef](#)]
23. Jensen, J.A.; Svendsen, N.B. Calculation of Pressure Fields from Arbitrarily Shaped, Apodized, and Excited Ultrasound Transducers. *IEEE Trans. Ultrason. Ferroelectr. Freq. Control* **1992**, *39*, 262–267. [[CrossRef](#)]
24. OK-Jensen, J.A. FIELD: A Program for Simulating Ultrasound Systems. *Med. Biol. Eng. Comput.* **1996**, *34*, 351–352.

25. Tortoli, P.; Bassi, L.; Boni, E.; Dallai, A.; Guidi, F.; Ricci, S. ULA-OP: An Advanced Open Platform for Ultrasound Research. *IEEE Trans. Ultrason. Ferroelectr. Freq. Control* **2009**, *56*, 2207–2216. [[CrossRef](#)] [[PubMed](#)]
26. Boni, E.; Bassi, L.; Dallai, A.; Guidi, F.; Ramalli, A.; Ricci, S.; Housden, J.; Tortoli, P. A Reconfigurable and Programmable FPGA-Based System for Nonstandard Ultrasound Methods. *IEEE Trans. Ultrason. Ferroelectr. Freq. Control* **2011**, *59*, 1378–1385. [[CrossRef](#)] [[PubMed](#)]
27. Boni, E.; Cellai, A.; Ramalli, A.; Tortoli, P. A high performance board for acquisition of 64-channel ultrasound RF data. In Proceedings of the 2012 International Ultrasonics Symposium, Dresden, Germany, 5–7 October 2012; pp. 2067–2070. [[CrossRef](#)]
28. Ramalli, A.; Guidi, F.; Boni, E.; Tortoli, P. A real-time chirp-coded imaging system with tissue attenuation compensation. *Ultrasonics* **2015**, *60*, 65–75. [[CrossRef](#)] [[PubMed](#)]
29. Golay, M. Complementary series. *IEEE Trans. Inf. Theory* **1961**, *7*, 82–87. [[CrossRef](#)]
30. Tseng, C.C.; Liu, C.L. Complementary Sets of Sequences. *IEEE Trans. Inf. Theory* **1972**, *18*, 644–652. [[CrossRef](#)]
31. Denarie, B.; Bjastad, T.; Torp, H. Multi-line transmission in 3-D with reduced crosstalk artifacts: A proof of concept study. *IEEE Trans. Ultrason. Ferroelectr. Freq. Control* **2013**, *60*, 1708–1718. [[CrossRef](#)] [[PubMed](#)]



© 2019 by the authors. Licensee MDPI, Basel, Switzerland. This article is an open access article distributed under the terms and conditions of the Creative Commons Attribution (CC BY) license (<http://creativecommons.org/licenses/by/4.0/>).